

# Modeling the impact of moulin shape on subglacial hydrology

Celia TRUNZ<sup>1</sup>, Matthew D. COVINGTON<sup>1</sup>, Kristin POINAR<sup>2</sup>,  
Lauren C. ANDREWS<sup>3</sup>, Jessica MEJIA<sup>2,4</sup>, Jason GULLEY<sup>4</sup>

<sup>1</sup>Geosciences Department, University of Arkansas, Fayetteville AR, USA

<sup>2</sup>Department of Geology, University at Buffalo, Buffalo NY, USA

<sup>3</sup>Global Modeling and Assimilation Office, NASA Goddard Space Flight Center, Greenbelt MD, USA

<sup>4</sup>Geosciences Department, University of South Florida, Tampa FL, USA

## Key Points:

- We use a single-conduit subglacial hydrological model to study how moulin size and shape affect subglacial water pressure.
- Subglacial water pressure dynamics are controlled by the moulin cross-sectional area only within the range of daily water level oscillations.
- The englacial void ratio in glacier hydrology models can be represented by the moulin volume within the daily water level oscillation range.

---

Corresponding author: Celia Trunz, [celia.trunz@gmail.com](mailto:celia.trunz@gmail.com)

## 16 Abstract

17 Subglacial models represent moulins as cylinders or cones, but field observations  
 18 suggest the upper part of moulins in the Greenland Ice Sheet have more complex shapes.  
 19 These more complex shapes should cause englacial water storage within moulins to vary  
 20 as a function of depth, a relationship not currently accounted for in models. Here, we  
 21 use a coupled englacial–subglacial conduit model to explore how moulin shape affects  
 22 depth-dependent moulin water storage and water pressure dynamics within a subglacial  
 23 channel. We simulate seven different moulin shapes across a range of moulin sizes. We  
 24 find that the englacial storage capacity at the water level is the main control over the  
 25 daily water level oscillation range and that depth-varying changes in englacial water stor-  
 26 age control the temporal shape of this oscillation. Further, the cross-sectional area of the  
 27 moulin within the daily oscillation range, but not above or below this range, controls pres-  
 28 sures within the connected subglacial channel. Specifically, large cross-sectional areas can  
 29 dampen daily to weekly oscillations that occur in the surface meltwater supply. Our find-  
 30 ings suggest that further knowledge of the shape of moulins around the equilibrium wa-  
 31 ter level would improve englacial storage parameterization in subglacial hydrological mod-  
 32 els and aid predictions of hydro-dynamic coupling.

## 33 Plain Language Summary

34 The speed of glacier ice flowing towards the ocean is influenced by timing and the  
 35 amount of water flowing in moulins. Moulins are large vertical shafts that penetrate the  
 36 entire ice thickness to transport water from the glacier’s surface to the bed. Water lev-  
 37 els within moulins reflect the water pressure within channels that form underneath the  
 38 glacier, transporting meltwater seaward. Most models that are used to simulate this wa-  
 39 ter flow under the ice assume that moulins are cylindrical, but in reality they are not.  
 40 In this study, we show that non-cylindrical moulins affect how the water level fluctuates  
 41 within moulins, and that what matters is the shape of the moulin within the range where  
 42 the water level oscillates.

## 43 1 Introduction

44 In land-terminating regions of the Greenland Ice Sheet, the response of the sub-  
 45 glacial drainage system to meltwater inputs is a primary influence on ice motion (e.g.,  
 46 Andrews et al., 2014; Hoffman et al., 2016; Schoof, 2010). Spatial (Banwell et al., 2016)  
 47 and temporal (Schoof, 2010) variability in supraglacial meltwater input affects subglacial  
 48 channel water pressures and ice motion. While pressures within subglacial channels tend  
 49 to control mid-melt-season ice motion, changes in the inefficient subglacial drainage sys-  
 50 tem can influence late-season slowdowns (Andrews et al., 2014; Hoffman et al., 2016; Mejia  
 51 et al., 2021).

52 Englacial storage exerts an important control on the pressure dynamics within the  
 53 subglacial drainage system (Flowers & Clarke, 2002). Storage must be included within  
 54 some subglacial models to produce realistic oscillation dynamics in channelized subglacial  
 55 drainage systems (Werder et al., 2013). Storage can affect both the distance over which  
 56 pressure variations will diffuse away from channels (Werder et al., 2013) and the rate of  
 57 water pressure rise after the melt season (Downs et al., 2018). Consequently, storage plays  
 58 a central role in the link between meltwater and ice motion.

59 Moulins collect nearly all of the supraglacial meltwater on the Greenland Ice Sheet  
 60 (Smith et al., 2015) and route this meltwater to the most efficient parts of the subglacial  
 61 drainage system (Gulley et al., 2012). By connecting to subglacial channels, subglacial  
 62 water pressures are modulated by the water stored within moulins (Banwell et al., 2016;  
 63 Werder et al., 2013). Moulins represent a potentially large percentage of the englacial

void space that is directly coupled to the subglacial system (Covington et al., 2020). Most subglacial hydrological models treat englacial storage as a spatially uniform and temporally constant model parameter, such as englacial void fraction (Bartholomaeus et al., 2011; Hewitt, 2013; Hoffman et al., 2016; Koziol & Arnold, 2018; Stevens et al., 2018; Sommers et al., 2018; Werder et al., 2013). However, limited exploration within moulines in alpine type glaciers (e.g. Gulley et al., 2009; Holmlund, 1988; Vallot, 1898; Vatne & Irvine-Fynn, 2016) and in Greenland (Bourseiller et al., 2002; Covington et al., 2020; Griselin, 1995; Lambertson, 2002; Moreau, 2009) suggests that moulines often have irregular shapes, where storage capacity varies substantially with depth.

In this study, we explore how moulin shape affects water level dynamics in moulines and subglacial channels in a Greenland-type ice sheet using the single-conduit model developed by Covington et al. (2020). Since relatively little is known about specific moulin shapes in Greenland, we explore a variety of generic shapes and discuss how they relate to field observations. In Section 3.1, we test how various moulin shapes affect the equilibration timescales of the subglacial system using a constant meltwater input to the moulin. In Section 3.2, we test how the shape of a moulin affects its response to diurnally varying meltwater input. We conclude by interpreting our simulation results in the context of the englacial void ratio, bed connectivity, and consequent ice velocity.

## 2 Model description

Diameter-evolving subglacial channels have been simulated in numerous prior studies (e.g. Röthlisberger, 1972; Schoof, 2010; Spring & Hutter, 1981) and can be coupled with a reservoir to include the storage of the moulin (Clarke, 1996; Covington et al., 2012; Werder et al., 2010). This type of model provides a simple and efficient physically based framework for studying the dynamics of an individual moulin-fed subglacial channel.

To explore the relationship between moulin shape and moulin water level variation, we employ a simplified model of the coupled englacial-subglacial hydrological system. The model contains a single subglacial channel that is fed by a vertical moulin (Figure 1a). The moulin collects meltwater input which is then evacuated through a subglacial channel. The moulin’s shape remains fixed throughout any single model run, with only the subglacial channel’s cross-sectional area ( $S$ ) allowed to evolve through melt and creep (Figure 1c), which are functions of subglacial discharge and effective pressure, respectively. Discharge and effective pressure vary with the height of the water column within the moulin’s shaft, which we represent as hydraulic head ( $h$ ). The rate of change of head ( $dh/dt$ ) depends on the difference between the discharge into ( $Q_{\text{in}}$ ) and out of ( $Q_{\text{out}}$ ) the moulin and the storage volume within the moulin. Importantly, storage is controlled by the cross-sectional area of the moulin at the water level,  $A_r(h)$ .

For this study, we implement the reservoir constriction model described in Covington et al. (2012) with the subglacial channel evolution model described in Schoof (2010), without the cavity component, as we assume the subglacial system is already channelized. The moulin component was adapted to allow the moulin cross-sectional area ( $A_r$ ) to vary with depth. The model is composed of two coupled differential equations simulating the time evolution of moulin head ( $h$ ) and the subglacial channel cross-sectional area ( $S$ ) at the entrance of the channel where the water exits the moulin. The rate of change of head ( $h$ ) within the moulin is given by

$$\frac{dh}{dt} = \frac{1}{A_r(h)} (Q_{\text{in}} - Q_{\text{out}}), \quad (1)$$

where  $A_r(h)$  is the cross-sectional area  $A_r$  of the moulin at  $h$ ,  $Q_{\text{in}}$  is the meltwater input into the moulin, and  $Q_{\text{out}}$  is the subglacial channel water output. Following Schoof (2010), we invoke the Darcy-Weisbach law,

$$Q_{\text{out}} = C_3 S^{5/4} \sqrt{\rho_w g h / L}, \quad (2)$$

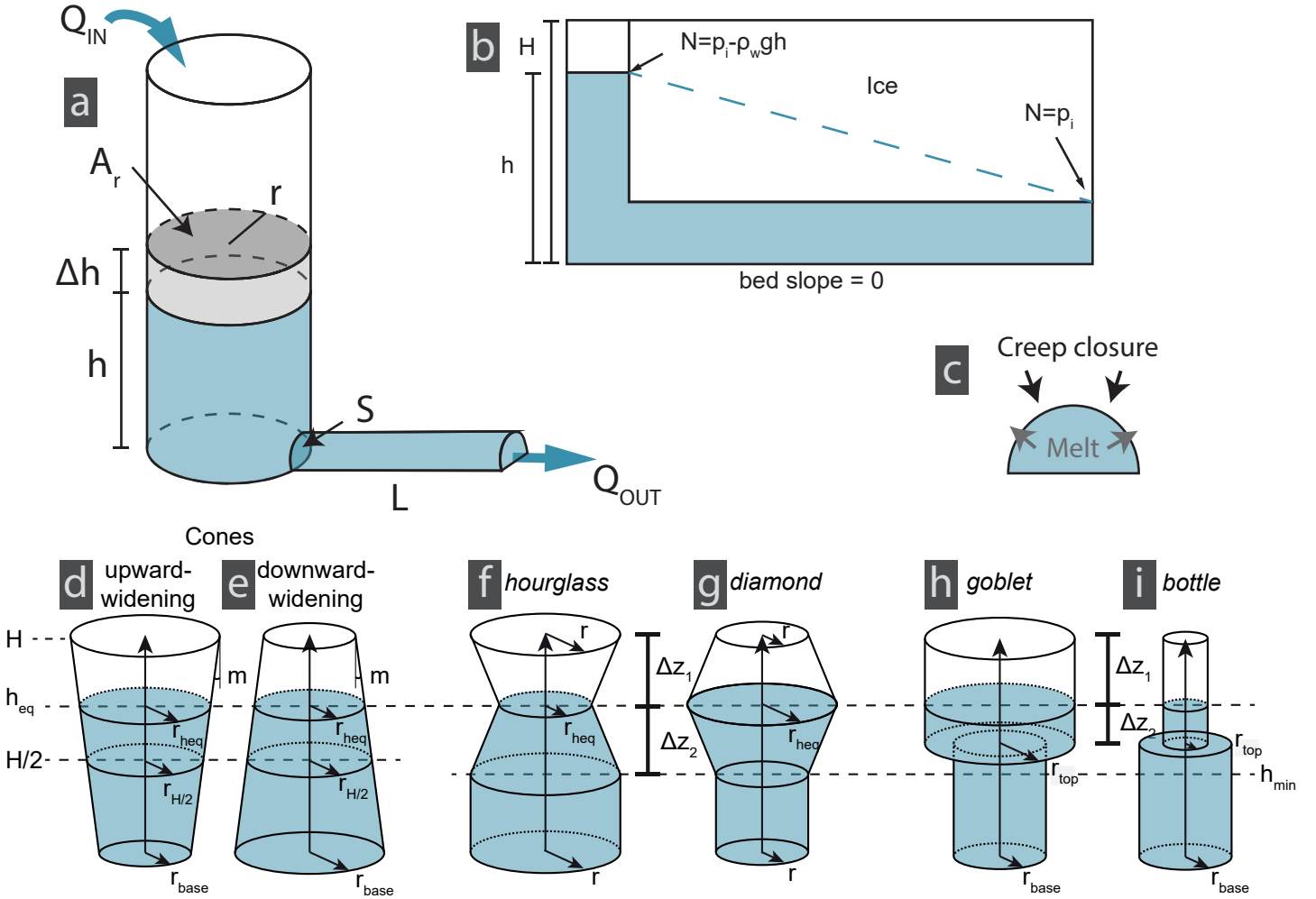


**Figure 1.** Schematic model diagrams. (a) Sketch of the model representing a moulin connected with a subglacial channel (Covington et al., 2012), with the meltwater input ( $Q_{in}$ ), discharge ( $Q_{out}$ ), moulin cross-sectional area ( $A_r$ ), moulin radius ( $r$ ), moulin head ( $h$ ), subglacial channel length ( $L$ ), and subglacial channel cross-sectional area ( $S$ ). (b) Longitudinal cross-section of the model. The effective pressure ( $N$ ) in the conduit at any point is the pressure of the ice ( $P_i$ ) minus the hydraulic head ( $\rho_w g h$ ) defined with the water density ( $\rho_w$ ), the gravity ( $g$ ) and the head ( $h$ ) relative to the bed. The blue dashed line represents the position of the water if we drilled a well in the subglacial channel. (c) The subglacial channel can creep closed or open depending on head and ice thickness adapted from (Schoof, 2010) (d-e) Cone-shaped moulin used for constant meltwater input simulations. We compare different cones by fixing the radius at the equilibrium head ( $h_{eq}$ ) or at half of the ice thickness ( $H/2$ ). The slope of the moulin wall is determined by  $m$  and is described in more detail in Supporting Text S2. (c-f) Moulin shapes used for the oscillating meltwater input simulations. We design the change in wall slope to be fixed at  $h_{eq}$  in (f) and (g), with  $Z_{hmin}$  just below the lowest water level in the set of simulations. The abrupt changes in radius in (h) and (i) are set to be between  $Z_{hmin}$  and  $Z_{heq}$ .

113 where  $L$  is the channel length or, equivalently, the distance between the moulin and the  
 114 ice-sheet margin for this simplified case of a single subglacial conduit. The variable  $\rho_w$   
 115 is the water density,  $g$  is the gravitational acceleration, and the flux parameter  $C_3 =$   
 116  $2^{5/4}\sqrt{\pi}/(\pi^{1/4}\sqrt{\pi+2\sqrt{\rho_w f}})$ , where  $f$  is the Darcy-Weisbach friction factor. The cou-  
 117 pled subglacial channel creep and melt equations are based on the Röthlisberger (1972)  
 118 and Nye (1976) description of R-channels and are given by

$$119 \quad \frac{dS}{dt} = C_1 C_3 S^{5/4} \left( \frac{\rho_w g h}{L} \right)^{3/2} - C_2 (P_i - \rho_w g h)^n S, \quad (3)$$

120 for the melt opening parameter  $C_1 = 1/(\rho_i L_f)$ , where  $L_f$  is the latent heat of fusion  
 121 and  $\rho_i$  is ice density. The viscous creep closure parameter is  $C_2 = Bn^{-n}$ , where  $B$  is  
 122 the Glen’s law fluidity coefficient and  $n$  is the Glen’s law exponent. The ice overburden  
 123 pressure is  $P_i = \rho_i g H$ , where  $H$  is the ice thickness.

124 The model makes the following assumptions (Figure 1: (1) bed slope is zero; (2)  
 125 the hydraulic gradient in the conduit is controlled by the large-scale ice sheet topogra-  
 126 phy; and (3) melt and creep dynamics within the channel are controlled by the water  
 127 pressure and ice thickness in the vicinity of the moulin; (4) water flow in the subglacial  
 128 channel is turbulent; and (5) water that enters the moulin leaves only through the sub-  
 129 glacial channel. For simplicity, we consider that all of the water transits through the chan-  
 130 nel; we do not account for loss or exchange of water with the distributed or weakly con-  
 131 nected parts of the subglacial system. The model is a 0-D or lumped model, therefore,  
 132 the cross-sectional area of the subglacial channel is represented by a single value.

133 While our model is a simplification of one part of the full subglacial hydrological  
 134 system, it contains all of the components required to explore relationships between moulin  
 135 storage and pressure variability within a subglacial channel without introducing unneces-  
 136 sary complexity and uncertain parameters. A variety of similar lumped models have  
 137 been used in previous studies (Arnold et al., 1998; Bartholomew et al., 2012; Clarke, 1996;  
 138 Covington et al., 2012, 2020; Cowton et al., 2016; Dow et al., 2014; Schoof, 2010; Stub-  
 139 blefield et al., 2019; Werder et al., 2010). Specifically, Stubblefield et al. (2019) demon-  
 140 strated that such a lumped model displays very similar dynamics to a more complex extended  
 141 channel model. We also test this assumption with a simulation comparing our  
 142 simple 0-D model to an extended 1-D conduit model (supporting Text S3 and Figure S6).  
 143 Limitations of our simplified modeling approach are discussed in more detail in Section  
 144 4.2.

## 145 2.1 Model setup

146 We use meltwater input rates in the range of estimated supraglacial stream discharges  
 147 in the ablation zone on the western flank of the Greenland Ice Sheet (Smith et al., 2015).  
 148 We run two broad classes of simulations. In the first set of simulations (Section 3.1), the  
 149 meltwater input  $Q_{in}$  is fixed at  $3 \text{ m}^3/\text{s}$  to test the equilibration of the subglacial system  
 150 in the case of an abrupt change in meltwater input conditions, free of the diurnal vari-  
 151 ations typical of field-observed supraglacial discharge, to isolate the internal system dy-  
 152 namics from any effects of time-varying forcing. In the second set of simulations (Sec-  
 153 tion 3.2–3.3), we use diurnally varying supraglacial meltwater input:

$$154 \quad Q_{in}(t) = Q_a \sin(2\pi t/P) + Q_{\text{mean}}, \quad (4)$$

155 where  $Q_{in}$  is meltwater input rate in function of time ( $t$ ).  $Q_{in}$  oscillates around a mean  
 156 meltwater input  $Q_{\text{mean}} = 3 \text{ m}^3/\text{s}$  with an amplitude ( $Q_a$ ) of  $0.4 \text{ m}^3/\text{s}$  and a period ( $P$ )  
 157 of one day. This diurnal range of moulin input is kept low to prevent the simulated wa-  
 158 ter level from overflowing. The simulations are run for an initialization period of 40 days,  
 159 until the amplitude of the daily oscillations stabilizes. This allows us to isolate the dy-  
 160 namics created by varying meltwater input, rather than the damped oscillations produced  
 161 during the equilibration of the system.

For most of the simulations (Section 3.1.1, 3.2–3.3), we use a single ice thickness of 1000 m, which is appropriate for a moulin 30 km away from the margin, to simulate moulin located within a single area of the ice sheet. We choose parameter values that are roughly representative of the field areas in Greenland where moulin water-level data are available (Andrews et al., 2014; Covington et al., 2020). By keeping the ice thickness constant across simulations, we are able to isolate the influence of different moulin shapes and meltwater input magnitudes on moulin water level and subglacial water pressures. For the simulations in Section 3.1.2, however, we test how the system behaves at different positions across the ice sheet. In order to scale the ice thickness at the moulin to a series of conduit lengths representative of the profile of a land-terminating glacier in Greenland, we use an idealized square root glacier (Hewitt et al., 2012), with zero ice thickness at the margin and 1000 m ice thickness at 30 km from the margin, defined by

$$H = 1 \text{ km} \sqrt{\frac{L}{30 \text{ km}}}, \quad (5)$$

where  $H$  is the ice thickness and  $L$  is again the subglacial channel length, equivalent to the distance between the moulin and the margin. This equation provides a single value of ice thickness in the vicinity of the moulin for each simulation with a given distance from the margin.

To explore the influence of moulin shape on subglacial water pressure dynamics, we use a series of idealized moulin shapes with geometries illustrated in Figure 1d–i. These shapes were chosen to cover a wide spectrum of possible moulin geometries because, to date, shapes of Greenland moulin in the region of summer water level fluctuations have not been mapped. We adapt the model of Covington et al. (2012) (Figure 1) by implementing a moulin with circular cross-sectional area with a depth-dependent radius (Clarke, 1996; Werder et al., 2010). We assume that the moulin has a circular cross-section and calculate the cross-sectional area  $A_r = \pi r^2$ , for a depth-dependent radius  $r$ . The slope of the wall ( $m$ ) is defined as  $m = dr/dz$ , where  $r$  is the moulin radius and  $z$  the elevation from the bed. The elevation difference  $\Delta z$  is calculated above the equilibrium head.

For specific simulation subsets, we compare moulin of different sizes and shapes with identical radii at either at the elevation of half of the ice thickness ( $H/2$ ) or at the equilibrium head ( $h_{\text{eq}}$ ). The equilibrium head (Röthlisberger, 1972) is introduced in Section 3 and is the altitude at which the water level in the moulin oscillates around, or stabilizes to, after a change in forcing. For the fixed meltwater input simulations (Section 3.1), we compare cone-shaped moulin (Figure 1d–e) of different sizes and shapes but identical radii at  $h_{\text{eq}}$  or identical radii at  $H/2$ . The parameterization is described in Supporting Text S2. For the oscillating meltwater input simulations (Section 3.2), we compare hourglass, diamond, goblet, and bottle-shaped moulin (Figure 1f–i). The parameterizations of moulin shapes are described in the Supporting Information (Figure S5).

### 3 Model experiments

#### 3.1 Model experiments with a fixed meltwater input

For a fixed rate of meltwater discharge within a subglacial channel, there exist equilibrium values for head ( $h_{\text{eq}}$ ) and channel diameter that can accommodate this discharge while simultaneously balancing the rates of wall melt and creep closure within the channel (Röthlisberger, 1972). If a channel is initialized at this state, then it will remain at equilibrium until the external forcing changes. When a subglacial channel is coupled to an englacial storage element, such as a moulin, the system can spontaneously oscillate around these values of equilibrium head and diameter, even with constant meltwater delivery (Clarke, 1996; Stubblefield et al., 2019). However, for the parameter space that we explore here, if our model is run with constant discharge and initialized sufficiently far from the equilibrium head and conduit diameter for that discharge, then it behaves

211 as a damped oscillator, which eventually approaches the equilibrium state (Supporting  
 212 Figure S1). Therefore, the system exhibits two inherent timescales: one associated with  
 213 the oscillation and one associated with the damping of the oscillations. We refer to the  
 214 latter as the equilibration timescale. Effectively, the equilibration timescale approximates  
 215 the time that is required for the system to evolve from one equilibrium state to another  
 216 after a change in forcing, such as the moulin discharge.

217 Here, we run two sets of constant meltwater input simulations. In the first set, we  
 218 fix parameters of ice thickness and channel length and explore the impact that moulin  
 219 shape has on the equilibration timescale (Section 3.1.1). In the second simulation set,  
 220 we systematically vary ice thickness and channel length for a subset of possible moulin  
 221 shapes (Section 3.1.2). We use this second set of simulations to examine whether sensi-  
 222 tivity to moulin shape varies across the ice sheet.

### 223 **3.1.1 Effect of moulin shape on equilibration timescales**

224 First, we examine the impact of moulin shape on equilibration timescale for fixed  
 225 ice thickness and conduit length. We run four subsets of simulations using four differ-  
 226 ent methods for varying moulin shapes. For the first subset, we use cylindrical moulins  
 227 and simply vary the moulin radius from 5 to 15 m (Figure 2 a–c), which is in the range  
 228 of radii observed in the field by (Covington et al., 2020). In the other three simulation  
 229 subsets, we use moulins with sloping walls that widen either upward or downward. For  
 230 the second subset, we employ a common moulin radius of 10 m at  $H/2$  (Figure 2 d–f).  
 231 For the third and fourth simulation subset, we fix the moulin radius to 10 m at  $h_{\text{eq}}$  (Fig-  
 232 ure 2 g–k). For the fourth simulation subset (Figure 2 j–k), however, we mirror the change  
 233 in wall slope around  $h_{\text{eq}}$  so that the radius at  $h_{\text{eq}}$  is either the smallest or the largest within  
 234 the range of water level oscillations. The wall slope,  $m$ , ranges from  $-2\%$  to  $+2\%$  for  
 235 the simulations with a common radius at  $H/2$ , and from  $-6\%$  to  $+6\%$  for the simula-  
 236 tions with a common radius at the equilibrium head elevation.

237 In the four sets of simulations shown in Figure 2, both head ( $h$ ) and subglacial cross-  
 238 sectional area at the moulin’s outlet ( $S$ ) have underdamped oscillations that reach an  
 239 equilibrium head of about 750 m above the bed. For the cylindrical subset (Figure 2a–  
 240 c), we observe that, for the same  $Q_{\text{in}}$  of  $3\text{ m}^3/\text{s}$ , head oscillations in the larger moulin  
 241 ( $r = 15\text{ m}$ ) decay with an e-folding time of 13 days and have an oscillation period of five  
 242 days, where the e-folding time is the time that it takes for the oscillation amplitude to  
 243 decay by a factor of  $e$ . The e-folding time for the decay of oscillations in the smaller moulin  
 244 ( $r = 5\text{ m}$ ) is about one day with a oscillation period of less than two days (Support-  
 245 ing Tables S2–S4). This is consistent with common reservoir-model behavior, wherein  
 246 the timescale for filling and draining increases with increasing reservoir size (e.g., Cov-  
 247 ington et al., 2009, 2012; Stubblefield et al., 2019).

248 In the simulation subset with cone-shaped moulins with radius fixed at  $H/2$  (Fig-  
 249 ure 2d–f) the shapes and total volumes of the moulins are quite different than for the  
 250 cylindrical cases. However, they display behavior that is similar to the cylindrical cases.  
 251 For example, an upward-widening cone with wall slope of  $+2\%$  from the vertical axis (pur-  
 252 ple line) has a low total storage capacity below the water line compared to a downward-  
 253 widening cone with the opposite wall slope ( $-2\%$ ; red line). However, we observe very  
 254 similar behavior in the time evolution of  $h$  and  $S$  as for cylindrical moulins, where equi-  
 255 libration time increases with moulin storage volume within the range of water level oscil-  
 256 lation. We probe this further using the third and fourth subset of modeled moulins,  
 257 where storage at  $h_{\text{eq}}$  is fixed with a radius of  $r = 10\text{ m}$  (Figure 2g–i and j–l). For the  
 258 third subset (Figure 2g–i), we observe that the timescales of both oscillation and equi-  
 259 libration are nearly identical from one moulin to another, regardless of wall slope. This  
 260 is true even for extreme cases of wall slope (Figure 2g–i, red and purple lines). Both  $h$   
 261 and  $S$  vary nearly identically as in the cylindrical (2c, black line) and cone  $H/2$  (2f, black

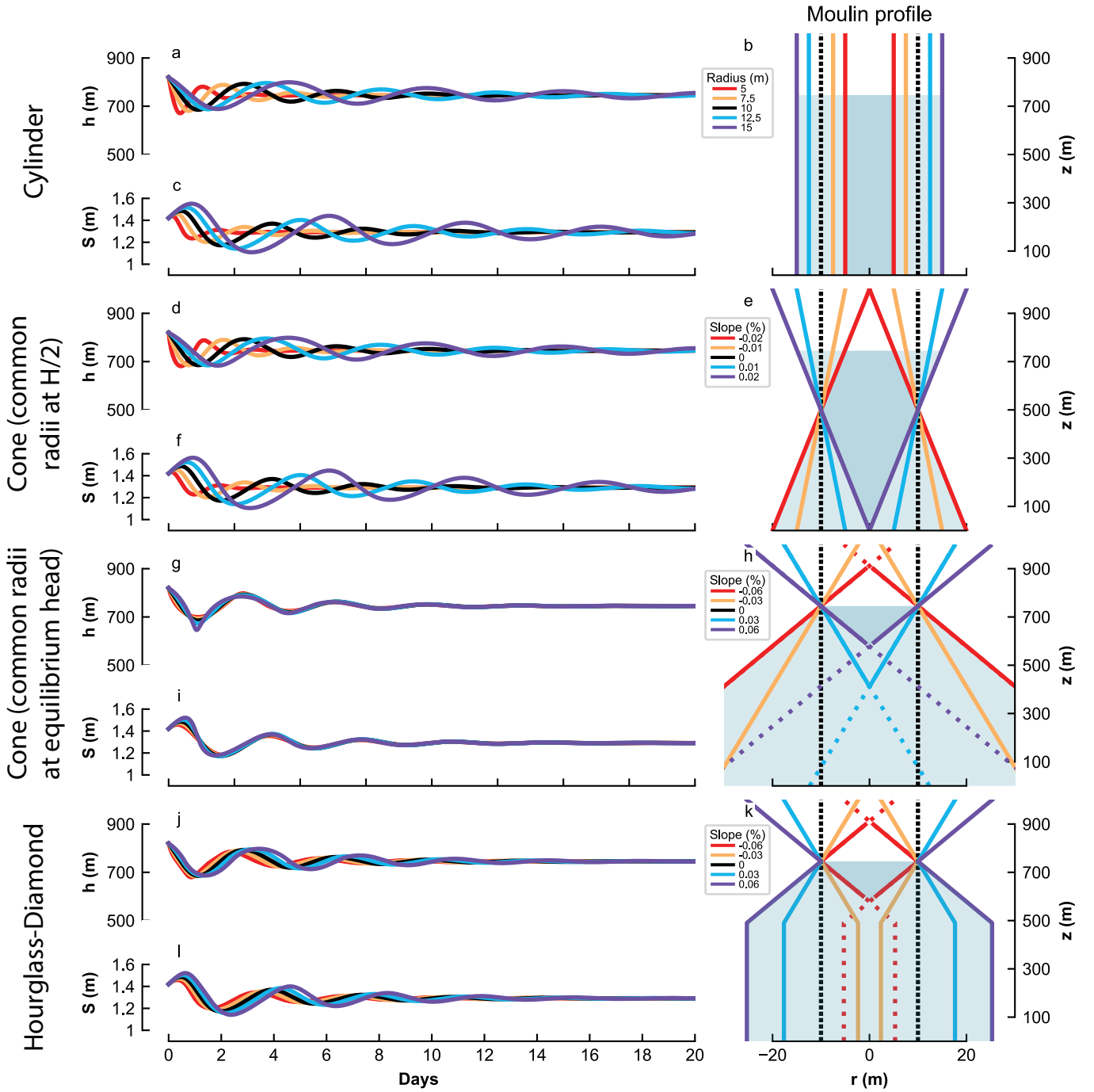


**Figure 2.** Equilibration timeseries of head ( $h$ ) and channel cross-sectional area ( $S$ ) simulated with a fixed meltwater input  $Q_{in}$  for various moulin shapes. For all simulations the length and thickness of the glacier is constant. Rows correspond to the following moulin shapes: cylindrical (a–c) with variable diameters, conical (d–i) with variable wall slopes with the radius held constant at an elevation of half the ice thickness (d–f) or at the equilibrium head altitude (g–i), and hourglass-diamond (j–l) centered around the equilibrium head altitude. For each shape, the timeseries of moulin head ( $h(m)$ ) and subglacial channel cross-sectional area ( $S$ ) are shown on the left. The moulin’s cross-sectional profile is on the right with dark blue and light blue illustrating water common to all moulins and water in a subset of moulins, respectively. The vertical axes of moulin profiles are at scale with head, but not with  $S$ . Model parameters are  $Q_{in} = 3 \text{ m}^3/\text{s}$ ,  $L = 30 \text{ km}$ ,  $H = 1000 \text{ m}$ .

line) cases that have  $r = 10$  m at  $h_{\text{eq}}$ . We observe a similar behavior for the fourth subset (Figure 2j–l), with a bit more variation in the equilibration timescales between the different simulations than for the cone-shaped moulin. The mirroring of the slope above and below  $h_{\text{eq}}$  increases the effect of wall slopes, since the change in area is either positive or negative during both high and low water. For the conical moulin, the opposite signs of the changes in area above and below equilibrium have a cancelling effect.

While the dynamical timescales are effectively the same for all the simulations with similar  $r(h_{\text{eq}})$ , the shape of the oscillations near the peaks and the troughs depends on wall slope (Figure 2g–h). The shape of the head extremum is rounder in Figure 2g (purple line) when the moulin widens in the direction of head displacement (red line), and more sharply peaked when the moulin narrows in that direction.

### 3.1.2 Equilibration timescales for different ice thicknesses

To examine if the equilibration timescale is sensitive to the moulin position on the ice sheet, we run a series of simulations for several positions along a profile of an idealized parabolic glacier (Figure 3) by systematically varying the parameters of  $H$  at the moulin and  $L$  from the moulin to margin. As before, each of these simulations uses a single ice thickness representative of the ice thickness near the moulin. The idealized glacier shape is only used to appropriately scale ice thickness at the moulin with distance from the margin. We use the same four classes of moulin shapes as in Section 3.1.1. For each shape class we compare the oscillation timescale ( $\tau_{\text{osc}}$ ), which represents the period of the underdamped fluctuations, and the damping timescale ( $\tau_{\text{damp}}$ ) which is the e-folding time over which the system equilibrates. We extract  $\tau_{\text{osc}}$  and  $\tau_{\text{damp}}$  of  $h$  and  $S$  by fitting the solution for a damped harmonic oscillator to our simulated timeseries (Supporting Figure S1), using

$$h(t) = ae^{-t/\tau_{\text{damp}}} \sin\left(\frac{2\pi}{\tau_{\text{osc}}}t + \phi\right) + h_{\text{eq}} \quad (6)$$

$$\phi = \begin{cases} \pi & \text{if } h(t=0) < h_{\text{eq}} \\ 0 & \text{if } h(t=0) > h_{\text{eq}} \end{cases} \quad (7)$$

where  $a$  is the amplitude,  $t$  is time, and  $\phi$  is the phase shift of the simulated timeseries.

For cylindrical moulin with the same meltwater input ( $Q_{\text{in}}$ ), we find that oscillation and damping timescales ( $\tau_{\text{osc}}$  and  $\tau_{\text{damp}}$ ) increase with distance from the margin and with increasing radius (Figure 3, first column). Note that  $\tau_{\text{osc}}$  in (Figure 3e–h) has high values close to the margin, where the damping of the head towards equilibrium is quicker than a full period of oscillation. Consequently, our fitting method for finding the equilibration timescales is likely less accurate close the margin. For cone-shaped moulin with common radii at  $H/2$  (Figure 3, second column), the timescales display an intersection point around 10 km from the margin, a distance that is specific to our parameter choices. Here, for downward-widening moulin, the timescales initially decrease with distance from the margin, because increases in the equilibrium head bring the water levels into a narrower portion of the moulin. For upward-widening moulin a similar, but opposite, effect enhances the increases in the timescales with distance from the margin. As a result,  $\tau_{\text{damp}}$  for a wall slope of 0.02 reaches a maximum of 15 days at 40km, where the moulin radius at the water level becomes disproportionately large compared to the meltwater input. Overall, these results illustrate that the diameter of the moulin at  $h_{\text{eq}}$  is the primary control on these timescales and that ice thickness has a secondary effect. This is further demonstrated by the simulations for cone-shaped and diamond-hourglass moulin with common radii at  $h_{\text{eq}}$  (Figure 3 right columns) which show reduced variation in  $\tau_{\text{osc}}$  and  $\tau_{\text{damp}}$  across moulin shapes, so long as the radius at  $h_{\text{eq}}$  is the same.

For these simulations, both timescales reflect mainly the position of the moulin on the ice sheet, not the moulin shape. Furthermore,  $\tau_{\text{osc}}$  and  $\tau_{\text{damp}}$  for all cone-shaped moulin

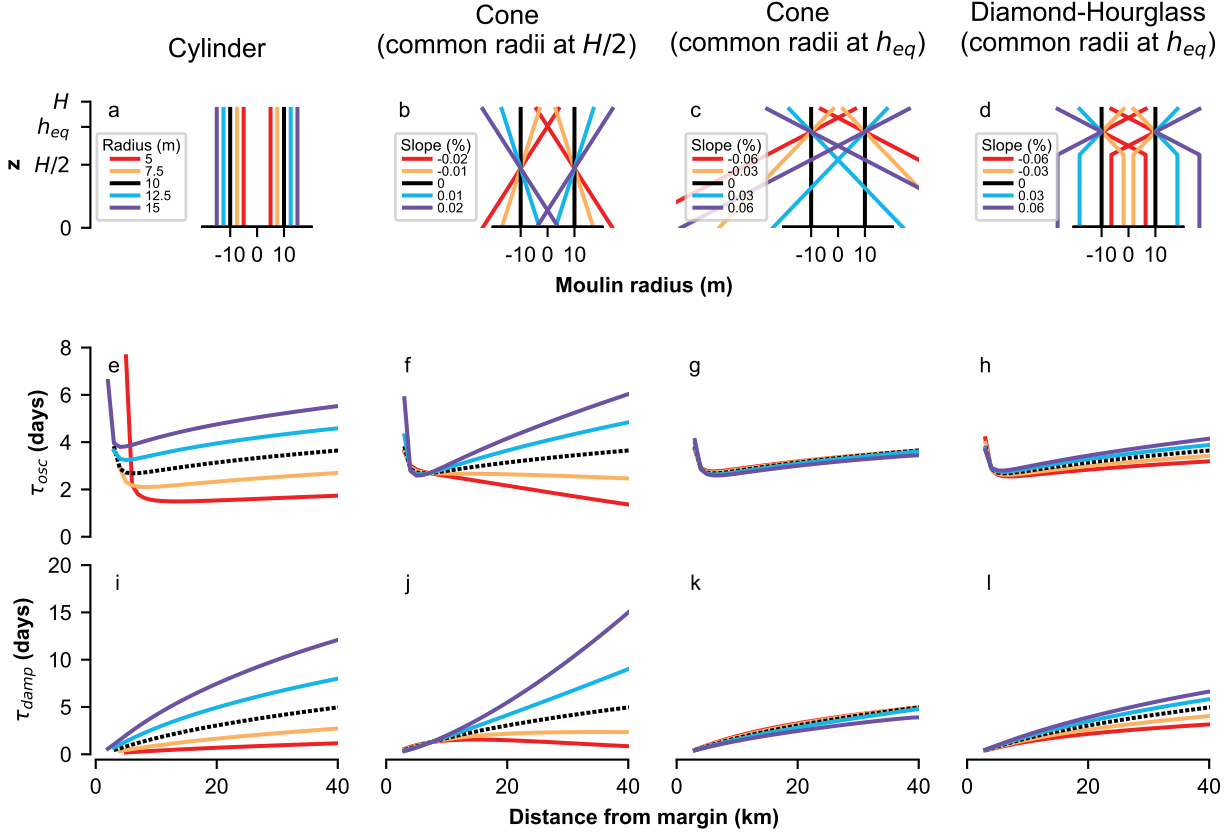


**Figure 3.** The equilibration timescales, along an idealized parabolic ice sheet profile (Equation 5) for cylindrical (a), conical (b–c), and hourglass-diamond (d) shaped moulins. The oscillation timescale ( $\tau_{osc}$ ) (e–h) represents the period of the underdamped fluctuations, while the damping timescale ( $\tau_{damp}$ ) (i–l) is the e-folding time over which the system reaches equilibrium. For a cylindrical moulin (left column), a cone-shaped moulins with a fixed radius at  $H/2$  (second column) and at  $h_{eq}$  (third column), and diamond-hourglass shaped moulins with a fixed radius at  $h_{eq}$  (right column).

310 in this subset are the same as that of the cylindrical moulin with a radius of 10 m, which  
 311 is equal to the radius of the cone-shaped moulins at  $h_{\text{eq}}$ . Therefore, we find that the moulin’s  
 312 cross-sectional area at  $h_{\text{eq}}$  controls the equilibration timescales.

### 313 3.2 Model experiments with an oscillating meltwater input

314 On glaciers and ice sheets, meltwater discharge flowing into moulins is not constant  
 315 in time but oscillates with changes in surface melt. In this section, we focus on the im-  
 316 pact of moulin shape on the dynamics of moulin water level and subglacial conduit cross-  
 317 sectional area under diurnally varying meltwater delivery.

318 We test a variety of simple, physically plausible shapes. We design these moulins  
 319 such that the changes in cross-sectional area are focused within the range of elevations  
 320 of water level oscillation. This is because we observe in Section 3.1 that only changes in  
 321 moulin shape around  $h_{\text{eq}}$  affect the head and subglacial channel size. We use two dif-  
 322 ferent approaches to vary moulin shape near  $h_{\text{eq}}$ . In the first approach, we vary the moulin  
 323 wall slope around  $h_{\text{eq}}$  (“hourglass”, “diamond”, Figure 1f,g) to keep our focus on the wall  
 324 slope and not on the change in cross-sectional area at  $h_{\text{eq}}$ . In the second approach, we  
 325 abruptly change the moulin cross-sectional area at  $h_{\text{eq}}$  (“goblet”, “bottle”, Figure 1h,i)  
 326 to mimic differential melting observed in moulins in the field. We compare results from  
 327 all of these runs to the cylindrical standard, for a total of five moulin shapes.

328 As noted in Section 3.1, moulin shapes do not have a strong influence on equili-  
 329 bration timescales; however, moulin shape does affect the amplitude and shape of the  
 330 peaks and troughs in head and subglacial channel cross-sectional area in response to os-  
 331 cillating meltwater input. In this simulation subset, we observe how the five tested shapes  
 332 affect the amplitude and shape of the oscillating responses in  $h$  and  $S$  for the same si-  
 333 nusoidal meltwater input.

334 We compare cylindrical moulins, with radii varying from 3.5 – 15 m (Figure 4a–  
 335 e), to hourglass- and diamond-shaped moulins with different wall slopes but with a com-  
 336 mon radius at one position in the moulin (Figure 4f–o), and to moulins with fixed wall  
 337 slopes with varying radius (Figure 4p–y).

338 For similar  $Q_{\text{in}}$ , the oscillation amplitudes of  $h$  and  $S$  are controlled by the moulin  
 339 volume within the oscillation range, similar to what was observed with a fixed input (Sec-  
 340 tion 3.1). The magnitude of  $A_r$  in the head oscillation range, whether depth-independent  
 341 (Figure 4a–e) or depth-varying (Figure 4f–y), strongly affects the amplitude of oscilla-  
 342 tions. For a given  $A_r$  at  $h_{\text{eq}}$ , a wall slope of just -2% from the vertical axis (Figure 4f–  
 343 j red) can double the oscillation amplitude compared to a cylinder. This is due to the  
 344 depth-dependent moulin volume within the oscillation range: the ability of the moulin  
 345 to store water decreases as  $h$  rises above  $h_{\text{eq}}$ , thus forcing a faster rise. This change in  
 346 oscillation amplitude is particularly pronounced above the equilibrium head, where in-  
 347 creases in radius at  $h_{\text{eq}}$  systematically reduce the amplitudes, regardless of the slope.

348 We observe asymmetry in both peak shape and the height of peaks versus depth  
 349 of troughs above and below equilibrium. This asymmetry is driven by the asymmetry  
 350 between the rates of melt and creep closure of the subglacial channel. In general, under  
 351 conditions typical of an ice sheet, the subglacial channel is able to close faster than it  
 352 can grow. This means that the subglacial channel closes quickly as meltwater input de-  
 353 creases and water pressure falls. But, when meltwater input increases, and the conduit  
 354 must reopen, the melt opening process is slower. Accordingly, the water level increases  
 355 faster than the conduit can accommodate, creating a large increase in water level in the  
 356 moulin.

357 To investigate the relationship between moulin water level variation and moulin  
 358 storage capacity, we use the dimensionless meltwater input frequency  $f^*$  from Covington

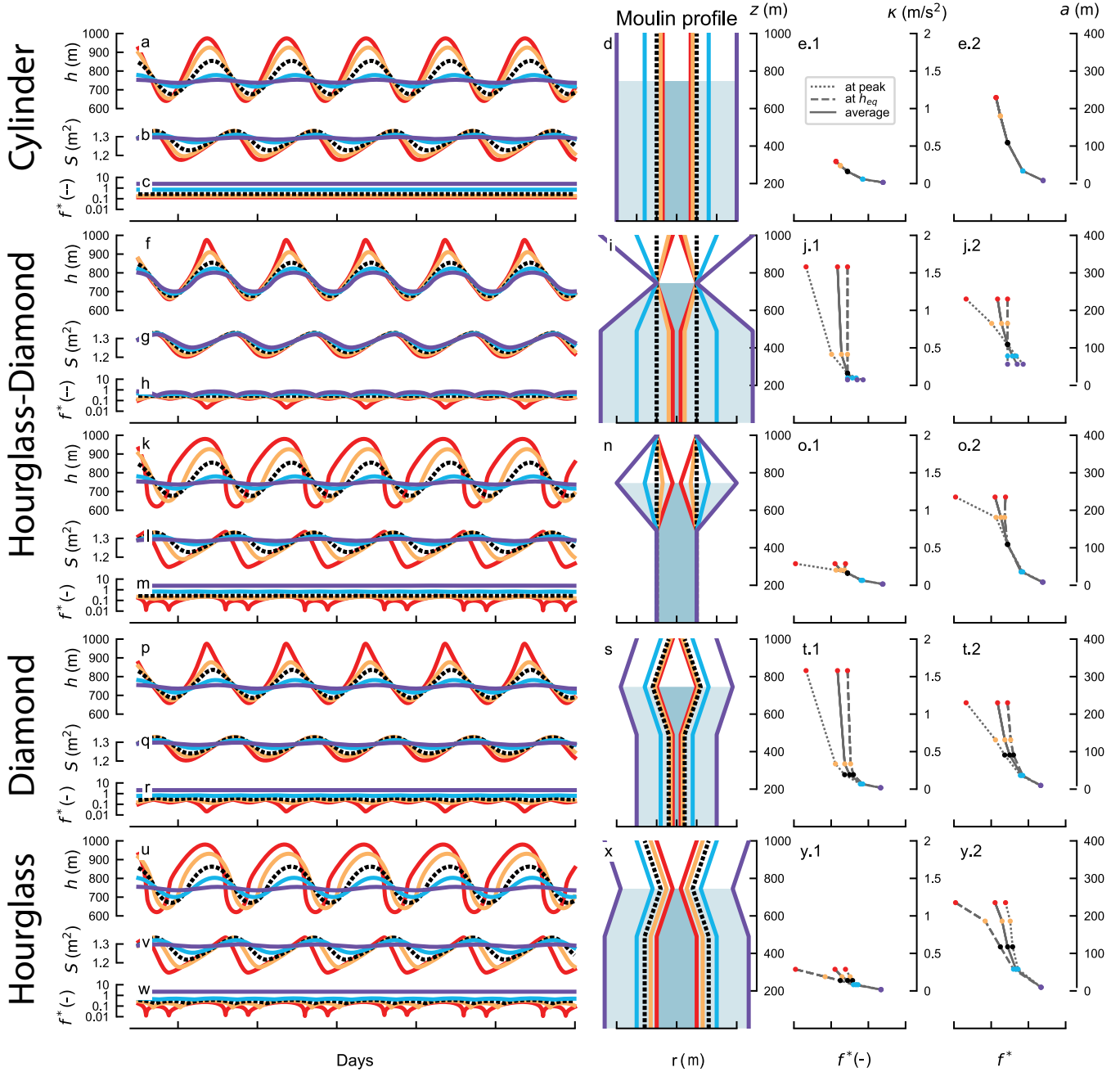


**Figure 4.** Timeseries of head ( $h$ ), channel cross-sectional area ( $S$ ), and dimensionless meltwater input frequency ( $f^*$ ), for a sinusoidal  $Q_{in}$  oscillating from 2.6 to 3.4 m<sup>3</sup>/s with a daily period for multiple idealized moulin shapes. For cylindrical moulin (a–e) the **radius** ( $r$ ) is uniform such that a large radius dampens oscillations in  $h$  and  $S$ , reducing  $f^*$  uniformly. For hourglass-diamond shaped moulin the radius is either fixed at  $h_{eq}$ , with varying wall slope above and below  $h_{eq}$  (f–j), or the radius is fixed above and below the water oscillation, and the radius varies at  $h_{eq}$  (k–o). For diamond-shaped (p–t) and hourglass-shaped (u–y) moulin the slope is fixed and the radius varies between model runs. Moulin profiles follow Fig (3). The correlation between **peakedness**,  $\kappa$ —represented by the second derivative of the head oscillation—and  $f^*$  (left) and the correlation between the **peak-to-peak amplitude of oscillation** ( $a$ ) and  $f^*$  (right) are shown for each moulin shape. Values corresponding to peak head (dash-dot), equilibrium head (dashed), and mean values (solid) are shown.

359 et al. (2020), which is the ratio of the time it takes for the moulin to fill to overburden  
 360 pressure and the duration of the meltwater input cycle:

$$361 \quad f^* = \frac{\tau_{fl}}{P_{osc}}, \quad (8)$$

362 where the period of oscillation of the meltwater input ( $P_{osc}$ ) is one day and the storage  
 363 timescale ( $\tau_{fl}$ ) is given by

$$364 \quad \tau_{fl} = \left( \frac{\rho_i}{\rho_w} \right) \frac{H A_r}{Q_{in}}, \quad (9)$$

365 where  $\rho_i$  and  $\rho_w$  are the density of ice and water, respectively,  $H$  is the ice thickness, and  
 366  $A_r$  is the moulin cross-sectional area. Essentially, a moulin acts as a low-pass filter, where  
 367 water storage filters out frequencies above  $f^* \gtrsim 1$ . For the cylindrical case, where  $A_r$   
 368 is depth-independent, so too is  $f^*$  (Figure 4c). For non-cylindrical moulins, however,  $f^*$   
 369 changes with head (Figure 4h,m,r,w). For these cases, we use local cross-sectional area  
 370 as a function of head,  $A_r(h)$ , to calculate  $f^*$  as a function of head.

371 For a cylindrical moulin, we find that when  $f^* > 1$  (Figure 4a–e, purple line), di-  
 372 urnal oscillations are almost completely filtered out, but they remain for  $f^* < 1$  (Fig-  
 373 ure 4c). For the diamond-shaped moulin (Figure 4r, yellow and red) the timeseries of  
 374  $f^*$  shows two pointy troughs per 24h period. The large and the small  $f^*$  troughs coin-  
 375 cide with the peaks and troughs, respectively, of  $h$ , where  $A_r$  reaches minima. The main  
 376 trough is due to the narrowing above  $h_{eq}$ , and the secondary trough is due to the nar-  
 377 rowing below  $h_{eq}$ . Even though the moulin shape is symmetric above and below  $h_{eq}$ , the  
 378 water level rises higher above  $h_{eq}$  than it falls below, due to the asymmetry caused by  
 379 subglacial melt-creep dynamics. For the hourglass shaped moulin, the twice-daily troughs  
 380 in  $f^*$  coincide with the subglacial channel cross-sectional extremum (Figure 4w). In this  
 381 case, the narrowest portion of the moulin is positioned at  $h_{eq}$ .

382 We hypothesize that variations in oscillation shape (amplitude and peakedness) are  
 383 controlled by the dimensionless meltwater input frequency ( $f^*$ ). To quantify the peaked-  
 384 ness ( $\kappa$ ) of the oscillations, we calculate the curvature of the timeseries in the vicinity  
 385 of the peak, using

$$386 \quad \kappa = \left. \frac{d^2 h}{dt^2} \right|_{\text{peak}}, \quad (10)$$

387 where larger curvature values will correspond to a sharper peak. Finally, we calculate  
 388 the amplitude ( $a$ ) of the oscillation above  $h_{eq}$  as

$$389 \quad a = h_{\text{peak}} - h_{\text{eq}}. \quad (11)$$

390 To test our hypothesis, we compare values of  $f^*$  at  $h_{eq}$  (dashed lines),  $h_{\text{peak}}$  (dotted-  
 391 dashed lines), and averaged (solid) against  $\kappa$  and  $a$  (Figure 4e,j,o,t,y). It is important  
 392 to keep in mind that for a specific  $H$  and  $Q_{in}$ , which here are held fixed,  $f^*$  is a direct  
 393 reflection of  $A_r$ . We find that the smallest value of  $f^*$  within the head oscillation range  
 394 controls the amplitude of oscillations if  $f^* < 1$  (Figure 4), while the peakedness is con-  
 395 trolled by  $f^*$  averaged (Figure 4p–t, red line). Additionally, when the trough in  $f^*$  cor-  
 396 responds to the equilibrium head (Figure 4h–y, red line), we observe deformation of the  
 397 head oscillation shape, but not a significant increase in  $\kappa$ . When the minimum values  
 398 of  $f^*$  coincide with a head maximum or minimum, the shapes of the peaks and troughs  
 399 become distorted. In other cases, when the troughs in  $f^*$  coincide with the water level  
 400 being at  $h_{eq}$ , then the shape distortion appears around the mean of the oscillation (Fig-  
 401 ure 4k–m, red line).

### 402 **3.3 Effect of abrupt change of moulin shape**

403 Next we investigate how an abrupt change in moulin shape at a prescribed depth  
 404 affects the oscillation dynamics. Field exploration of moulins in Greenland (Covington

405 et al., 2020; Reynaud & Moreau, 1994; Moreau, 2009) has found ledges in some moulins,  
406 or large subaerial volumes that narrow at the water line. To represent these moulins sim-  
407 ply, we design goblet and bottle-shaped moulins that comprise two stacked cylinders of  
408 different radii (Figure 5f–j). We use these moulins to explore a hypothetical large change  
409 in volume above  $h_{\text{eq}}$  or just below the lowest head (Figure 5k–o).

410 First, we test how the equilibration timescales are affected by an abrupt change in  
411 shape. In contrast to the lack of impact of moulin wall slope (Figure 2g–i), we find that  
412 abrupt enlargement or reduction of moulin size at  $h_{\text{eq}}$  substantially changes the oscil-  
413 lation and damping timescales for the same meltwater input. We find that bottle-shaped  
414 moulins have faster equilibration timescales than cylindrical moulins, while hourglass-  
415 shaped moulins require more time for the head to equilibrate (Supporting Figure S3).

416 We also test how this abrupt change in volume affects the head oscillations with  
417 diurnally varying meltwater input (Figure 5). We find that abrupt changes in moulin ra-  
418 dius around  $h_{\text{eq}}$  affect the amplitudes of the oscillations in  $h$  and  $S$ . This is despite the  
419 fact that all moulins had an identical radii for some 60% of the depth. An increase of  
420 the moulin radius by just one meter (10%) reduced the amplitude of the water oscilla-  
421 tions by a third (Figure 5f–j, black and blue lines), suggesting that strongly dampened  
422 water level oscillations can occur in moulins with a wide chamber above the water line,  
423 regardless of their shape below the water line. In contrast, goblet and bottle-shaped moulins  
424 in which the cylinders of different radii join below the oscillation range (Figure 5k–o) do  
425 not show variations in the pattern or amplitude of water oscillation. These final simu-  
426 lations illustrate that water level oscillations are insensitive to static storage volumes that  
427 are always below the water level.

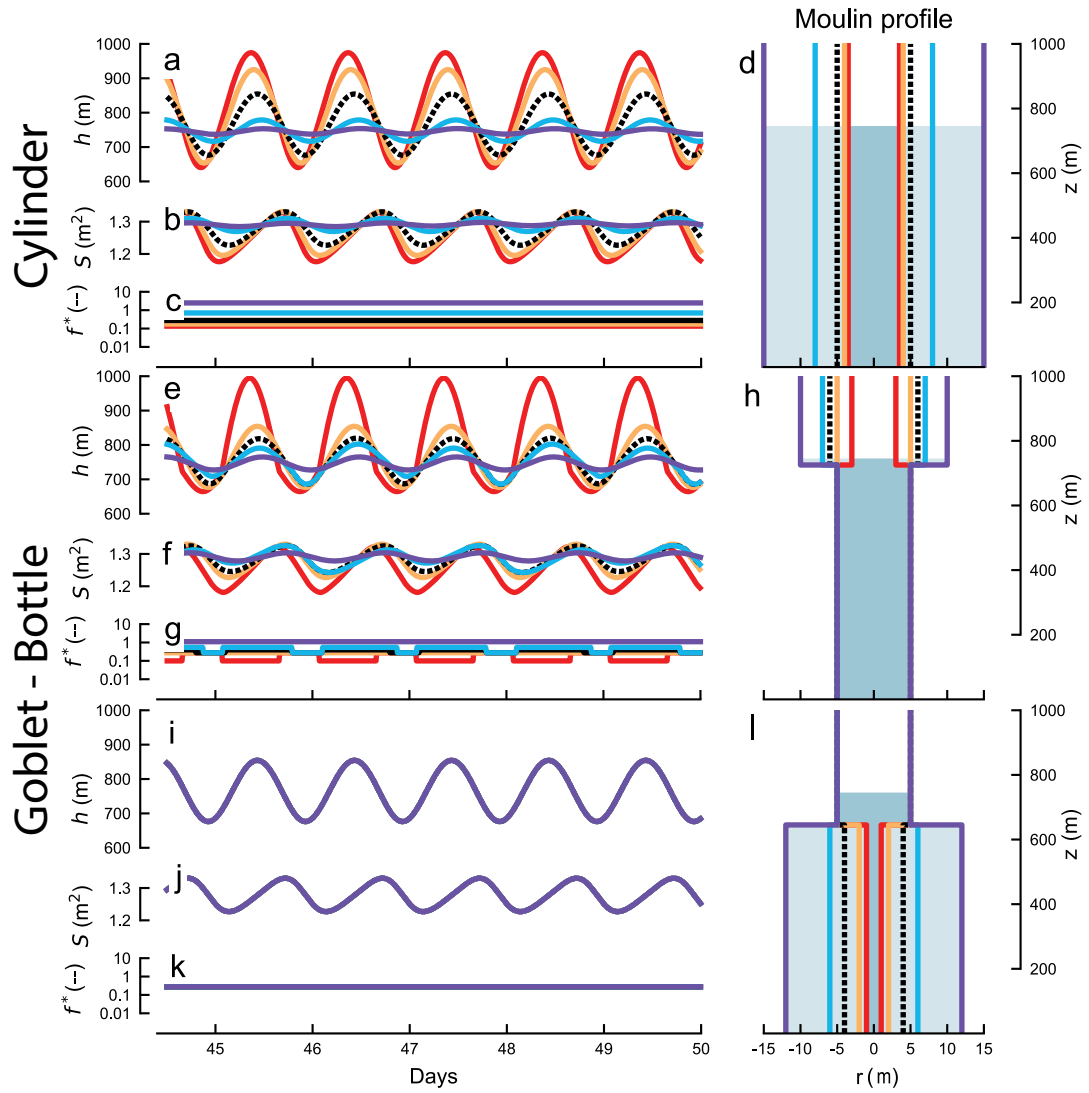


**Figure 5.** Timeseries of head ( $h$ ), channel cross-sectional area ( $S$ ), and dimensionless meltwater input frequency ( $f^*$ ), for a daily sinusoidal  $Q_{in}$  oscillating from  $2.6$  to  $3.4 \text{ m}^3/\text{s}$  for multiple idealized moulin shapes: Cylindrical (a–d), goblet-bottle-shaped with radius fixed below (e–h) and above (i–l) the equilibrium head ( $h_{eq}$ ).

## 4 Discussion

### 4.1 Controls on head variability

Moulin storage modulates changes in subglacial pressure by regulating variations in moulin hydraulic head (Andrews et al., 2021; Covington et al., 2012, 2020). Here, we examine how vertical changes in moulin storage impact the amplitude and form of moulin head oscillations. Moulins act as low-pass filters between meltwater inputs at the surface and englacial discharge into the subglacial system, removing high-frequency oscillations and transmitting low-frequency oscillations. This low-pass filter behavior can be quantified using the dimensionless oscillation frequency,  $f^*$ , where oscillations that occur on timescales where  $f^* \gtrsim 1$  will be strongly damped.

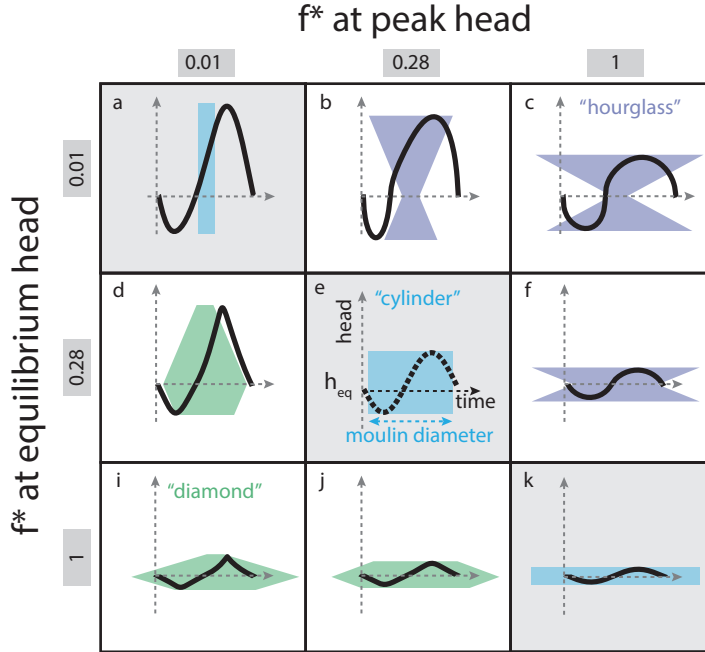


**Figure 6.** The amplitudes and shapes of moulin head ( $h$ ) oscillations for selected dimensionless meltwater input frequency ( $f^*$ ) at peak head ( $h_{\text{peak}}$ ) and at equilibrium head ( $h_{\text{eq}}$ ). Black lines show a single period of head oscillation. Blue shading shows the moulin shape within the range of water level oscillation. Moulin shapes are scaled consistently against the head timeseries and with one another. All moulin shapes are symmetric about  $h_{\text{eq}}$ . Values of  $f^*$  are highlighted in grey.

The storage that impacts the head oscillations in the moulin is the storage within which the head varies. We define "dynamic storage" as the storage that is filling and draining, and "static storage" as the storage that is always full of water. Note storage that is static at the daily timescale could be dynamic at a longer timescale. The impact of dynamic storage on the water level patterns that we observe can be categorized using the values of  $f^*$  at the equilibrium head elevation,  $f^*(h_{\text{eq}})$ , and at the peak head elevation,  $f^*(h_{\text{peak}})$ . We generalize these patterns of behavior in Figure 6, where we display selected 24 h head oscillations for specific choices of  $f^*(h_{\text{eq}})$  and  $f^*(h_{\text{peak}})$ .

Cylindrical moulin cases are depicted along the diagonal of Figure 6(a,e,k), where one can see the effect of increases in dimensionless meltwater input frequency leading to decreases in oscillation amplitude. However, oscillation amplitude also decreases if mov-

449 ing along an axis of increasing  $f^*(h_{\text{eq}})$  or increasing  $f^*(h_{\text{peak}})$  (Figure 6b,c,f), suggest-  
 450 ing that average  $f^*$  within the range of oscillation is responsible for controlling ampli-  
 451 tude. The peakedness of moulin head oscillations is controlled by whether  $f^*$  decreases  
 452 or increases as the water level approaches a peak or trough. Diamond-shaped moulins,  
 453 which fall below the diagonal in Figure 6, and have  $f^*(h_{\text{eq}}) > f^*(h_{\text{peak}})$ , produce sharply  
 454 peaked oscillations. Hourglass-shaped moulins, which are located above the diagonal in  
 455 Figure 6, and have  $f^*(h_{\text{eq}}) < f^*(h_{\text{peak}})$ , produce rounded oscillations. For the diamond-  
 456 shaped cases, cross-sectional area decreases towards the peaks and troughs. These de-  
 457 creases in  $A_r$  drive an increase in the rate of change in head, leading to sharpening of  
 458 the peaks. Similarly, if  $A_r$  increases towards peaks and troughs, then the rate of change  
 459 in head will be reduced near peaks and troughs, producing rounded peaks. In addition  
 460 to the low-pass filter behavior of moulins, changes in storage with depth can alter the  
 461 temporal shapes of water level oscillations. Therefore, it may be possible to constrain  
 462 the shapes of moulins by using a timeseries of moulin water levels observed in the field.

## 463 4.2 Influence of model assumptions on simulation results

464 The simplification of the subglacial channel model to an ordinary differential equa-  
 465 tion is based on the assumptions that (1) the hydraulic gradient is set by the large-scale  
 466 topography of the ice sheet, which can be approximated by  $h/L$ , and (2) that changes  
 467 in flow resistance are controlled by the cross-sectional area of the subglacial channel near  
 468 the moulin. The first assumption is based on the long and relatively flat topography of  
 469 the ice sheet, and the fact that the hydraulic grade line within subglacial conduits tends  
 470 to roughly follow the glacier topography (Röthlisberger, 1972). The second assumption  
 471 is based on the idea that the largest variations in water flow resistance in the subglacial  
 472 channel occur near the moulin, because the ice is thickest there and the discharge fluc-  
 473 tuations are the largest. In a recent lake drainage modeling study, Stubblefield et al. (2019)  
 474 demonstrated that the usage of simplified coupled ordinary differential equations (ODEs),  
 475 similar to the ones we use, instead of more complex partial differential equations (PDEs),  
 476 is sufficient for simulating pressure dynamics, while saving considerable computing time  
 477 and reducing parameter complexity.

478 We also compared the outputs from a more complex PDE model, where the chan-  
 479 nel can evolve along the horizontal axis, against our lumped ODE model (Supporting  
 480 Text S3 and Figure S6). We found that using the more complex model did not signif-  
 481 icantly change the water level dynamics (less than 10% of the ice thickness). However,  
 482 the mean water level is somewhat different in the two simulations, a result of the simpli-  
 483 fying assumptions in our ODE model. In the ODE model, the hydraulic gradient is  
 484 likely to be a bit steeper than it would be in reality, effectively increasing the flow for  
 485 a given hydraulic head and conduit cross-sectional area,  $S$ . On the other hand, the av-  
 486 erage  $S$  is likely to be underestimated, as we use a value representative of where the ice  
 487 thickness is the largest. In reality, we expect  $S$  to increase as the ice thickness decreases  
 488 along the conduit toward the margin. The smaller  $S$  in our ODE model would effectively  
 489 decrease flow for a given hydraulic head, somewhat countering the influence of the other  
 490 assumption. However, these two effects do not quite balance, resulting in the slight dif-  
 491 ferences in mean head values in the discretized (PDE) and lumped (ODE) conduit mod-  
 492 els. However, as we are interested in the relative change in water level induced by dif-  
 493 ferent moulin shapes, rather than the absolute head values, the simplified representa-  
 494 tion of the subglacial conduit in our model does not have a substantial influence on our  
 495 conclusions.

496 A second important simplification of the model is that it does not have a distributed  
 497 network, which in reality could exchange water with the subglacial channel. We might  
 498 expect such exchange flows with a distributed network to reduce the amplitude of os-  
 499 cillation of the head in the moulin. However, observed water levels in moulins in Green-  
 500 land rarely reach pressures observed in the unchanneled portion (Andrews et al., 2014;

501 Covington et al., 2020; Mejia et al., 2021; Meierbachtol et al., 2013; Wright et al., 2016),  
 502 which is necessary for the water to be pushed into the distributed network. Furthermore,  
 503 daily changes in storage volumes within the distributed network are limited, again sug-  
 504 gesting that they would not have a substantial impact on moulin water level dynamics  
 505 (Covington et al., 2020).

506 Arguably, one of the most limiting assumptions in our model is its representation  
 507 of the englacial–subglacial system as a single moulin connected to a single channel, rather  
 508 than a network. In reality, moulins will interact with other nearby moulins, such that  
 509 the shape of a single moulin will not be the only driving factor of head variation (Andrews  
 510 et al., 2014, 2021). Moulin water level dynamics will likely average over storage avail-  
 511 able in nearby moulins that are tightly coupled through the conduit network. Also, we  
 512 might expect some background discharge from other moulins or basal melt that could  
 513 provide a baseflow discharge that reduces oscillation amplitude (Andrews et al., 2021;  
 514 Trunz, 2021). While such effects are likely to influence moulin water level dynamics in  
 515 nature, the model presented here is sufficient to explore the relative impact of moulin  
 516 shape on the amplitude of oscillation.

### 517 **4.3 Potential shapes of Greenland Ice Sheet moulins**

518 Here we have used idealized shapes to explore, in general, how moulin shape can  
 519 influence subglacial water pressure dynamics. However, real-world moulins are likely to  
 520 display a somewhat narrower range of shapes than we modeled. In general, moulins will  
 521 evolve through a combination of melt due to turbulent flow of water and viscous and elas-  
 522 tic deformation of the ice (Andrews et al., 2021; Catania & Neumann, 2010; Poinar et  
 523 al., 2017). Is it not clear, however, whether moulins often evolve to an equilibrium form  
 524 or whether moulin lifetimes are sufficiently short that they are abandoned before the drivers  
 525 of expansion and contraction can reach a balance. However, the size of a moulin should  
 526 be correlated to the size of the supraglacial stream feeding it. This likely restricts plau-  
 527 sible ranges of  $f^*$ , which depends linearly on moulin volume and inversely on meltwa-  
 528 ter discharge.

529 The limited field observations inside the Greenland Ice Sheet (Covington et al., 2020;  
 530 Reynaud & Moreau, 1994) have not yet extended beyond the upper 10–20% of the ice  
 531 thickness, because moulins have been water filled below that depth at the time of ex-  
 532 ploration. Water levels in the fall, when exploration is possible, may also be somewhat  
 533 higher than average summer water levels and geometries may be modified due to the in-  
 534 creased creep closure rates. Some observed moulins also have ranges of water level os-  
 535 cillation that are much larger than the explored thicknesses (Andrews et al., 2014), high-  
 536 lighting additional uncertainty on moulin shapes within the relevant range of water level  
 537 oscillations. Nevertheless, observations in the upper parts of moulins suggest that gob-  
 538 let shapes may be more plausible than bottle shapes. Some explored moulins are roughly  
 539 cylindrical with a reduction of diameter at the water line, as observed in a moulin nearby  
 540 the the FOXX moulin (monitored by Andrews et al. (2014) and explored by Covington  
 541 et al. (2020)) and in the Isortoq moulin (Reynaud & Moreau, 1994). Phobos moulin was  
 542 roughly goblet-shaped, with a large chamber just above the water level (Covington et  
 543 al., 2020). We use the bottle shape moulin here as an end-member case to understand  
 544 how head dynamics relate to moulin shape, but it is unclear what physical processes could  
 545 produce such a shape. Phobos moulin did narrow substantially near the ice surface, but  
 546 it is unknown whether water levels would ever reach that elevation because the water  
 547 level measured in the nearby Radical moulin remained below 225 meters depth (Covington  
 548 et al., 2020) throughout the 2017 melt season.

549 Goblet-shaped moulins could be produced by differential melting of the walls, with  
 550 more melt above the equilibrium water level than below, or by strong creep closure of  
 551 the ice at depth. Field observations show that moulins tend to form in pre-existing crevasses

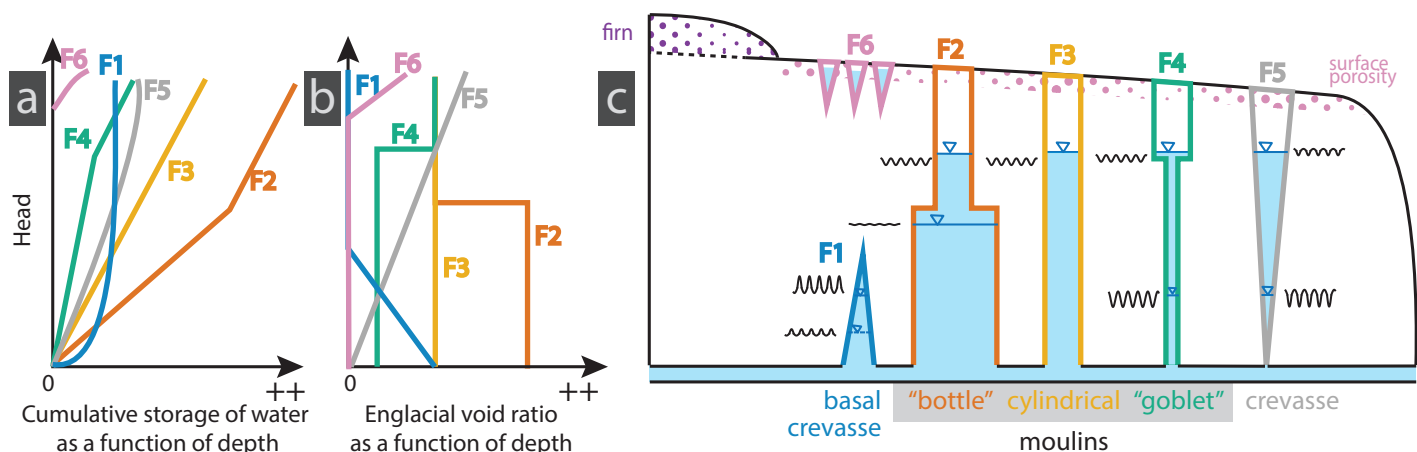


**Figure 7.** Conceptual sketch of englacial storage and englacial void ratio as a function of depth for idealized moulin shapes. The total stored water (a) gradually increases with increases in head, while the englacial void ratio (b) only changes when the radius of the moulin changes. (c) Representations of moulin profiles plotted in (a) and (b). Black oscillating timeseries depict the amplitude of water level oscillations in moulin when the water is at a specific depth. Oscillation amplitude is not a function of total moulin/englacial storage, but the dynamic storage, which is localized within the range of head oscillation.

552 or shear fractures (King, 2018; Smith et al., 2015). Such crevasses or fractures could also  
 553 create zones of preferential melt, wherein waterfall erosion processes and supraglacial stream  
 554 knickpoints could more rapidly enlarge moulin cross-sections. Because creep closure is  
 555 relatively slow in the top 100 meters of an ice column, these goblet shapes should tend  
 556 to be available for reuse from year to year (Catania et al., 2008). It is unclear if reused  
 557 moulins provide more storage than newly formed moulins, as the moulin partially creeps  
 558 closed at the end of the melt season. More field observations and modeling are neces-  
 559 sary to fully understand the processes that control moulin shapes.

#### 560 4.4 Implications for large-scale glacier hydrological models

561 To more accurately simulate subglacial pressure amplitudes in the efficient portion  
 562 of the subglacial drainage system, subglacial hydrological models often use an englacial  
 563 void parameter. The englacial void parameter accounts for the transient storage of water  
 564 in the englacial system (Flowers & Clarke, 2002). Englacial storage of water connected  
 565 to the bed will influence the amplitude and the timing of peak subglacial water pressure.  
 566 Moulins may be the most important englacial storage component, as they are directly  
 567 connected to both the subglacial and supraglacial channels (Covington et al., 2020). The  
 568 englacial void ratio or englacial void fraction parameter, is typically calculated as the  
 569 volume of void space divided by the volume of ice (Downs et al., 2018; De Fleurian et  
 570 al., 2018; Flowers, 2015). Although overall storage in the glacier is important on longer  
 571 timescales, we find that it is only the storage or englacial void ratio within the head os-  
 572 cillation range, which we call the dynamic storage, that affects the water level dynam-  
 573 ics in the efficient portion of the bed on a daily timescale.

574 As we find that the head oscillation amplitudes are strongly affected by dynamic  
 575 storage, we reflect here on the extent to which different types of englacial storage con-  
 576 tribute to this dynamic storage. We compare five shapes to illustrate how total water  
 577 storage and local englacial storage vary with depth (Figure 7, englacial storage elements

are numbered from F1 to F6). Moulins sketched in Figure 7(F2–F4) show that even though they have very different total storage capacities, they could induce similar head oscillation ranges if the water level is close to their tops (upper sinusoids). In the case of much lower water levels, though, the moulins would create very different oscillations (lower sinusoids). The high dynamic storage in moulin F2 will dampen oscillations, whereas the low dynamic storage in moulin F4 will enable large oscillations. Crevasses (Figure 7-F5) connected to a moulin (Colgan et al., 2011) could provide a substantial extra volume that could dampen oscillation amplitudes and filter out high frequency variation. Without such a connection, crevasses could provide long term storage at seasonal timescales (McGrath et al., 2011). Basal crevasses (F1 in Figure 7), if they are connected to the channelized system, would only influence the oscillation dynamics if the water level was below the top of the crevasse. They have been found in drilling (Harper et al., 2010) and seem to be present when basal water pressures are above overburden pressure (van der Veen, 1998). Therefore, they may be more likely in the weakly connected portion of the bed that has higher water pressure than the channelized system (Andrews et al., 2014; Wright et al., 2016). The firn aquifer, the surface crevasses, and the porosity at the surface (F6), while they could delay the arrival of meltwater to the moulin, are storage elements that are completely decoupled from basal water pressure, as they are not typically directly connected with the subglacial hydrological system (Downs et al., 2018; Hewitt, 2013).

Models typically treat storage as homogeneous, and therefore independent of vertical position (Banwell et al., 2016; Flowers & Clarke, 2002; Flowers, 2015; De Fleurian et al., 2018). However, storage is a function of depth (Figure 7). We find that the storage volume, or englacial void, that will affect basal water pressure dynamics in the channelized and surrounding distributed portions of the bed is the volume of moulins and connected crevasses within the range of head variation. The equilibrium head  $h_{eq}$  in a moulin (Meierbachtol et al., 2013; Röthlisberger, 1972), which is not influenced by the moulin shape but by the glacier characteristics (e.g. ice thickness, subglacial channel length) and the rate of discharge, can be predicted and is shown in Supporting Figure S4 for a wide range of mean meltwater inputs. The size and shape of the storage volume near equilibrium head, which is expected to be up to a few hundreds of meters below the surface, likely controls the amplitude and shape of daily head oscillation and has the ability to filter out meltwater variability with sufficiently high frequency ( $f^* \gtrsim 1$ ). Because moulins are directly connected to the efficient channelized system, the dynamic portion of the moulin may represent a substantial percentage of the englacial void ratio used in subglacial hydrology models.

#### 4.5 The impact of moulin shape on subglacial connectivity and ice speed

While this study investigates how moulin shape modulates water pressures within idealized subglacial channels, we use our results to infer how moulin shape might influence sliding speeds on seasonal timescales. Observed late melt season slowdowns have been attributed to the dewatering of isolated or weakly connected cavities (Andrews et al., 2014; Hoffman et al., 2016) Here, we consider the potential role of moulin shape in this dewatering process by comparing goblet and bottle-shaped moulins to the standard cylindrical shape (Figure 8), which all have the same radius at the equilibrium head  $h_{eq}$ .

When compared to a cylindrical moulin (Figure 8a), a goblet-shaped moulin with the same radius at and below the equilibrium head (Figure 8b) will have smaller diurnal water level oscillations, whereas a bottle-shaped moulin (Figure 8c) will have larger oscillations. Larger amplitude water level oscillations should induce stronger subglacial water pressure gradients, forcing water further out into the neighboring distributed drainage system. This could potentially lower pressures within a larger number of weakly connected cavities and connect a larger portion of the surrounding distributed system (Figure 8c). On the other hand, a moulin with smaller oscillations would have less ability to grow connectivity within the surrounding bed.

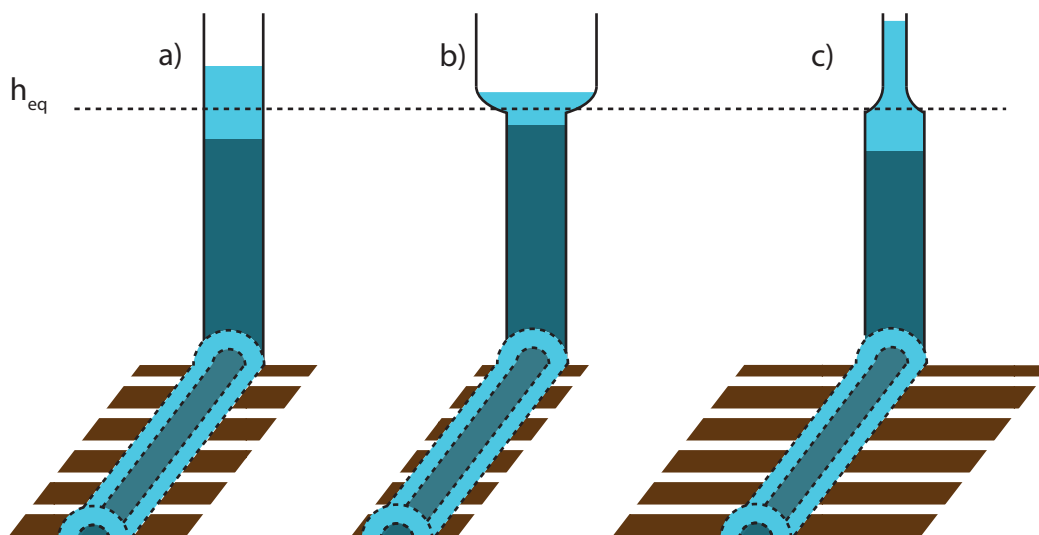


**Figure 8.** A comparison of the oscillation range for three example moulin shapes and the potential impact on the weakly connected portion of the bed. Light and dark blue indicate the ranges of oscillation in moulin water level and cross-sectional area of the subglacial channel. The brown striations represent the spatial range of influence of the moulin over the surrounding weakly connected bed, with larger pressure oscillations leading to a larger area of influence.

630 As long-term ice velocities are thought to relate to the weakly connected portion  
 631 of the bed, short-term pressure variability may play an important part in determining  
 632 whether early melt season increases in sliding speeds are offset by slowdowns later in the  
 633 melt season. Our results show that moulin shape and size influence pressure variability.  
 634 To offer stronger constraints on the impact of moulins over ice-sheet scales, more infor-  
 635 mation is needed on the sizes and shapes of moulins and whether they differ systemat-  
 636 ically across the ice sheet.

#### 637 **4.6 Complementary approaches to constraining the role of moulins on** 638 **ice-sheet hydrology**

639 We have shown that equilibration timescales, oscillation amplitude and shape, as  
 640 well as short-term englacial storage are affected only by volume and changes in volume  
 641 with height within the head oscillation range. Therefore, characterizing the shapes of the  
 642 upper portions of moulins will provide constraints for model storage parameters and aid  
 643 in interpretation of field data.

644 In order to appropriately represent the englacial storage directly connected to the  
 645 subglacial channel system, we need to determine not only the moulin density and dis-  
 646 tribution that can be estimated from satellite imagery (Phillips et al., 2011; Smith et al.,  
 647 2015), but also the geometry of moulins below the surface. However, if non-cylindrical  
 648 moulins are prevalent, it may not be possible to infer the cross-sectional areas of moulins  
 649 relevant for dynamic storage from satellite imagery, or even from surface observations,  
 650 since volumes at depth may be very different than those observed at the surface. Moulin  
 651 exploration is difficult, but continued mapping of moulins could provide precious data  
 652 to constrain the plausible range of dynamic storage volumes within the Greenland Ice  
 653 Sheet. While exploration and mapping of moulins will provide needed initial informa-  
 654 tion on the typical sizes and shapes of moulins and the factors that influence them, the  
 655 resources needed in such exploration will limit the number of moulins that can be ex-

656 plored. Therefore, it is also necessary to understand the processes that lead to the cre-  
657 ation of different shapes by modeling of moulin evolution. In this study, we simulated  
658 water level within moulins with a static shape. The time evolution and lifetimes of moulins  
659 will also likely influence how moulins modulate subglacial water pressures. A physically  
660 based model for moulin evolution, informed by field observations from moulin exploration  
661 could provide the information needed to extrapolate dynamic storage volumes across an  
662 ice sheet scale.

663 Finally, the model we use represents a single moulin connected to a single chan-  
664 nel. In reality, moulins are connected to a network of subglacial channels, exchanging  
665 and regulating meltwater inputs with each other. Therefore, understanding how a com-  
666 plex network of moulins interacts will be necessary to get a full picture of the impact of  
667 moulins on subglacial pressures. Since prior observations of nearby moulin water levels  
668 suggest rapid equilibration of heads through the subglacial system (Andrews et al., 2014),  
669 it seems likely that the dynamic storage governing water pressure variability represents  
670 an areally-averaged storage volume across many coupled moulins within a region of the  
671 ice sheet.

## 672 5 Conclusion

673 We use a simplified model of a subglacial conduit coupled to a moulin to explore  
674 relationships between moulin shape and head variation. Our results show that the shape  
675 of the moulin within the range of water level oscillations is the main control on the tem-  
676 poral pattern of head dynamics. More specifically, the size of the moulin at and around  
677 the equilibrium head position controls the amplitude of the oscillations, while the shape  
678 of the moulin controls the shape of the peaks and troughs in water level. We show that  
679 the englacial void parameter, used to account for englacial storage in glacial hydrolog-  
680 ical modeling, can be quantified by moulin volumes at and around  $h_{\text{eq}}$  (dynamic stor-  
681 age), and not by the overall volume of water held in moulins within a glacier (static stor-  
682 age).

683 In addition, we find that the dynamic storage of moulins dictates the magnitude  
684 of subglacial pressure increases associated with short-term perturbations in supraglacial  
685 runoff. The presence of large voids just above the equilibrium head position can strongly  
686 dampen the head oscillation amplitudes, even if the rest of the moulin has a relatively  
687 small diameter. Such small-amplitude oscillations may inhibit the growth of connectiv-  
688 ity within the surrounding weakly connected bed and potentially reduce the mid-to-late-  
689 season ice sheet slow down caused by sustained large meltwater inputs to the bed. Fu-  
690 ture modeling or mapping of moulins would enable better constraints on realistic ranges  
691 for dynamic storage within moulins and the controls on that storage, and therefore would  
692 improve understanding of the impact of meltwater on ice motion.

## 693 Notation

694	$h$	Moulin hydraulic head
695	$S$	Subglacial channel cross-sectional area
696	$h_{\text{eq}}$	Moulin equilibrium hydraulic head
697	$dh/dt$	Rate of change of head over time
698	$r$	Moulin radius
699	$r_{\text{heq}}$	Moulin radius
700	$r_{\text{top}}$	Moulin radius at the top of the moulin
701	$r_{\text{base}}$	Moulin radius at the base of the moulin
702	$r$	Moulin radius
703	$A_r$	Moulin cross-sectional area
704	$A_r(h)$	Moulin cross-sectional area at the water level
705	$Q_{\text{in}}$	Supraglacial meltwater input
706	$Q_{\text{out}}$	Subglacial channel water output
707	$Q_a$	Amplitude of oscillation of the meltwater input
708	$Q_{\text{mean}}$	Mean meltwater input
709	$H$	Ice thickness
710	$H/2$	Half of the ice thickness
711	$L$	Subglacial channel length
712	$z$	Elevation from bedrock
713	$m$	Moulin wall slope $\Delta r/\Delta z$
714	$\tau_{\text{osc}}$	Period of oscillation timescale
715	$\tau_{\text{damp}}$	Damping E-folding timescale
716	$f^*$	Non-dimensional meltwater input frequency
717	$a$	Amplitude of the moulin head oscillation above $h_{\text{eq}}$
718	$\kappa$	Peakedness of the moulin head oscillation in the vicinity of the peak

## 719 6 Open Research

720 The code (in Python) used to make the simulations and create the figures is avail-  
 721 able in the public Github repository [https://github.com/cctrnz/ModelRepo\\_MoulinShapeStoragePaper](https://github.com/cctrnz/ModelRepo_MoulinShapeStoragePaper)  
 722 `.git`. The current version of the model repository is the release v.2 (Trunz, 2022) and  
 723 is archived by Zenodo <https://zenodo.org/record/6338955>.

## 724 Acknowledgments

725 C.T., M.D.C., J.M., and J.G. were supported by the United States National Science Foun-  
 726 dation grants 1604022. K.P. and L.C.A. received support from NASA Cryosphere award  
 727 80NSSC19K0054. The authors declare there are no conflicts of interest with regard to  
 728 finances or with the results of this paper.

## 729 References

- 730 Andrews, L. C., Catania, G. A., Hoffman, M., Gulley, J., Lüthi, M. P., Ryser, C.,  
 731 ... Neumann, T. A. (2014). Direct observations of evolving subglacial  
 732 drainage beneath the Greenland Ice Sheet. *Nature*, 514(7520), 80–83. doi:  
 733 10.1038/nature13796
- 734 Andrews, L. C., Poinar, K., & Trunz, C. (2021). Controls on Greenland moulin ge-  
 735 ometry and evolution from the Moulin Shape model. *The Cryosphere Discus-*  
 736 *sions*, 1–47. doi: doi.org/10.5194/tc-2021-41
- 737 Arnold, N., Richards, K., Willis, I., & Sharp, M. (1998). Initial results from a dis-  
 738 tributed, physically based model of glacier hydrology. *Hydrological Processes*,

- 739 12(2), 191–219.
- 740 Banwell, A., Hewitt, I., Willis, I., & Arnold, N. (2016). Moulin density controls  
741 drainage development beneath the Greenland ice sheet. *Journal of Geophysical*  
742 *Research: Earth Surface*, 121(12), 2248–2269. doi: 10.1002/2015JF003801
- 743 Bartholomew, T. C., Anderson, R. S., & Anderson, S. P. (2011). Growth and  
744 collapse of the distributed subglacial hydrologic system of Kennicott Glacier,  
745 Alaska, USA, and its effects on basal motion. *Journal of Glaciology*, 57(206),  
746 985–1002. doi: 10.3189/002214311798843269
- 747 Bartholomew, I., Nienow, P., Sole, A., Mair, D., Cowton, T., & King, M. A. (2012).  
748 Short-term variability in Greenland Ice Sheet motion forced by time-varying  
749 meltwater drainage: Implications for the relationship between subglacial  
750 drainage system behavior and ice velocity. *Journal of Geophysical Research:*  
751 *Earth Surface*, 117(3), F03002. doi: 10.1029/2011JF002220
- 752 Bourseiller, P., Lambertson, J., Moreau, L., Couté, A., & Quennehen, C. (2002). *Voy-*  
753 *age dans les glaces*. Paris: La Martinière Jeunesse.
- 754 Catania, G. A., & Neumann, T. A. (2010). Persistent englacial drainage features in  
755 the Greenland Ice Sheet. *Geophysical Research Letters*, 37(2), L02501. doi: 10  
756 .1029/2009GL041108
- 757 Catania, G. A., Neumann, T. A., & Price, S. F. (2008). Characterizing englacial  
758 drainage in the ablation zone of the Greenland ice sheet. *Journal of Glaciol-*  
759 *ogy*, 54(187), 567–578. doi: 10.3189/002214308786570854
- 760 Clarke, G. K. C. (1996). Lumped-element analysis of subglacial hydraulic circuits.  
761 *Journal of Geophysical Research: Solid Earth*, 101(B8), 17547–17559. doi: 10  
762 .1029/96JB01508
- 763 Colgan, W., Steffen, K., McLamb, W. S., Abdalati, W., Rajaram, H., Motyka, R.,  
764 ... Anderson, R. (2011). An increase in crevasse extent, West Greenland:  
765 Hydrologic implications. *Geophysical Research Letters*, 38(18), L18502. doi:  
766 10.1029/2011GL048491
- 767 Covington, M. D., Banwell, A., Gulley, J., Saar, M. O., Willis, I., & Wicks, C. M.  
768 (2012). Quantifying the effects of glacier conduit geometry and recharge  
769 on proglacial hydrograph form. *Journal of Hydrology*, 414, 59–71. doi:  
770 10.1016/j.jhydrol.2011.10.027
- 771 Covington, M. D., Gulley, J. D., Trunz, C., Mejia, J., & Gadd, W. (2020). Moulin  
772 Volumes Regulate Subglacial Water Pressure on the Greenland Ice Sheet. *Geo-*  
773 *physical Research Letters*, 47(20). doi: 10.1029/2020GL088901
- 774 Covington, M. D., Wicks, C. M., & Saar, M. O. (2009). A dimensionless num-  
775 ber describing the effects of recharge and geometry on discharge from sim-  
776 ple karstic aquifers. *Water Resources Research*, 45(11), W11410. doi:  
777 10.1029/2009WR008004
- 778 Cowton, T., Nienow, P., Sole, A., Bartholomew, I., & Mair, D. (2016). Variabil-  
779 ity in ice motion at a land-terminating Greenlandic outlet glacier: the role of  
780 channelized and distributed drainage systems. *Journal of Glaciology*, 62(233),  
781 451–466. doi: 10.1017/jog.2016.36
- 782 De Fleurian, B., Werder, M. A., Beyer, S., Brinkerhoff, D. J., Delaney, I., Dow,  
783 C. F., ... Sommers, A. N. (2018). SHMIP The subglacial hydrology model  
784 intercomparison Project. *Journal of Glaciology*, 64(248), 897–916. doi:  
785 10.1017/jog.2018.78
- 786 Dow, C. F., Kulesa, B., Rutt, I. C., Doyle, S. H., & Hubbard, A. (2014). Up-  
787 per bounds on subglacial channel development for interior regions of the  
788 Greenland ice sheet. *Journal of Glaciology*, 60(224), 1044–1052. doi:  
789 10.3189/2014JoG14J093
- 790 Downs, J. Z., Johnson, J. V., Harper, J. T., Meierbachtol, T., & Werder, M. A.  
791 (2018). Dynamic Hydraulic Conductivity Reconciles Mismatch Between Mod-  
792 eled and Observed Winter Subglacial Water Pressure. *Journal of Geophysical*  
793 *Research: Earth Surface*, 123(4), 818–836. doi: 10.1002/2017JF004522

- 794 Flowers, G. E. (2015). Modelling water flow under glaciers and ice sheets. *Proc. R.*  
795 *Soc. A*, *471*(2176), 20140907. doi: 10.1098/rspa.2014.0907
- 796 Flowers, G. E., & Clarke, G. K. C. (2002). A multicomponent coupled model of  
797 glacier hydrology 1. Theory and synthetic examples. *Journal of Geophysical*  
798 *Research: Solid Earth*, *107*(B11), 2287. doi: 10.1029/2001JB001122
- 799 Griselin, M. (1995). *3e symposium international, cavités glaciaires et cryokarst en*  
800 *régions polaires et de haute montagne: Chamonix-France, 1er-6 novembre 1994*  
801 *: actes*. Presses Univ. Franche-Comté.
- 802 Gulley, J., Benn, D., Sreaton, E., & Martin, J. (2009). Mechanisms of englacial con-  
803 duit formation and their implications for subglacial recharge. *Quaternary Sci-*  
804 *ence Reviews*, *28*(19-20), 1984–1999. doi: 10.1016/j.quascirev.2009.04.002
- 805 Gulley, J., Walthard, P., Martin, J., Banwell, A., Benn, D., & Catania, G. (2012).  
806 Conduit roughness and dye-trace breakthrough curves: why slow velocity  
807 and high dispersivity may not reflect flow in distributed systems. *Journal of*  
808 *Glaciology*, *58*(211), 915–925. doi: 10.3189/2012JoG11J115
- 809 Harper, J. T., Bradford, J. H., Humphrey, N. F., & Meierbachtol, T. W. (2010).  
810 Vertical extension of the subglacial drainage system into basal crevasses. *Nat-*  
811 *ure; London*, *467*(7315), 579–82. doi: 10.1038/nature09398
- 812 Hewitt, I. (2013). Seasonal changes in ice sheet motion due to melt water lubrica-  
813 tion. *Earth and Planetary Science Letters*, *371-372*, 16–25. doi: 10.1016/j.epsl  
814 .2013.04.022
- 815 Hewitt, I., Schoof, C., & Werder, M. A. (2012). Flotation and free surface flow in a  
816 model for subglacial drainage. Part 2. Channel flow. *Journal of Fluid Mechan-*  
817 *ics*, *702*, 157–187. doi: 10.1017/jfm.2012.166
- 818 Hoffman, M., Andrews, L. C., Price, S. A., Catania, G. A., Neumann, T. A., Luthi,  
819 M. P., ... Morriss, B. (2016). Greenland subglacial drainage evolution reg-  
820 ulated by weakly connected regions of the bed. *Nature Communications*,  
821 *7*(13903). doi: 10.1038/ncomms13903
- 822 Holmlund, P. (1988). Internal Geometry and Evolution of Moulins, Stor-  
823 glaciären, Sweden. *Journal of Glaciology*, *34*(117), 242–248. doi: 10.1017/  
824 S0022143000032305
- 825 King, L. A. (2018). *Identifying and characterizing the spatial variability of*  
826 *supraglacial hydrological features on the western Greenland Ice Sheet* (Doc-  
827 toral dissertation, University of British Columbia). doi: 10.14288/1.0372827
- 828 Koziol, C. P., & Arnold, N. (2018). Modelling seasonal meltwater forcing of the  
829 velocity of land-terminating margins of the Greenland Ice Sheet. *Cryosphere*,  
830 *12*(3), 971–991. doi: 10.5194/tc-12-971-2018
- 831 Lambertson, J. (2002). *Les moulins de glace: mémoires d'un glacionaute*. Paris:  
832 Hoëbeke.
- 833 McGrath, D., Colgan, W., Steffen, K., Lauffenburger, P., & Balog, J. (2011). As-  
834 sessing the summer water budget of a moulin basin in the Sermeq Avannarleq  
835 ablation region, Greenland ice sheet. *Journal of Glaciology*, *57*(205), 954–964.  
836 doi: 10.3189/002214311798043735
- 837 Meierbachtol, T., Harper, J., & Humphrey, N. (2013). Basal Drainage System  
838 Response to Increasing Surface Melt on the Greenland Ice Sheet. *Science*,  
839 *341*(6147), 777–779. doi: 10.1126/science.1235905
- 840 Mejia, J. Z., Gulley, J. D., Trunz, C., Covington, M. D., Bartholomaus, T. C., Xie,  
841 S., & Dixon, T. H. (2021). Isolated Cavities Dominate Greenland Ice Sheet  
842 Dynamic Response to Lake Drainage. *Geophysical Research Letters*, *48*(19),  
843 e2021GL094762. doi: 10.1029/2021GL094762
- 844 Moreau, L. (2009). L'exploration du cryokarst glaciaire et son intérêt scien-  
845 tifique pour l'étude du drainage des eaux de fonte : porches, cavités, crevasses,  
846 bédrières et moulins. *Collection EDYTEM. Cahiers de géographie*, *8*(1), 163–  
847 170. doi: 10.3406/edyte.2009.1083
- 848 Nye, J. F. (1976). Water Flow in Glaciers: Jökulhlaups, Tunnels and Veins. *Journal*

- 849        *of Glaciology*, 17(76), 181–207. doi: 10.3189/S002214300001354X
- 850 Phillips, T., Leyk, S., Rajaram, H., Colgan, W., Abdalati, W., McGrath, D., & Stef-  
851 fen, K. (2011). Modeling moulin distribution on Sermeq Avannarleq glacier  
852 using ASTER and WorldView imagery and fuzzy set theory. *Remote Sensing*  
853 *of Environment*, 115(9), 2292–2301. doi: 10.1016/j.rse.2011.04.029
- 854 Poinar, K., Joughin, I., Lilien, D., Brucker, L., Kehrl, L., & Nowicki, S. (2017).  
855 Drainage of Southeast Greenland Firn Aquifer Water through Crevasses to the  
856 Bed. *Frontiers in Earth Science*, 5. doi: 10.3389/feart.2017.00005
- 857 Reynaud, L., & Moreau, L. (1994). Moulins glaciaires des glaciers tempérés et froids  
858 de 1986 à 1994 (Mer de Glace et Groenland) : morphologie et techniques de  
859 mesures de la déformation de la glace. Paris.
- 860 Röthlisberger, H. (1972). Water Pressure in Intra- and Subglacial Channels. *Journal*  
861 *of Glaciology*, 11(62), 177–203. doi: 10.1017/S0022143000022188
- 862 Schoof, C. (2010). Ice-sheet acceleration driven by melt supply variability. *Nature*,  
863 468(7325), 803–806. doi: 10.1038/nature09618
- 864 Smith, L. C., Chu, V. W., Yang, K., Gleason, C. J., Pitcher, L. H., Rennermalm,  
865 A. K., ... Balog, J. (2015). Efficient meltwater drainage through supraglacial  
866 streams and rivers on the southwest Greenland ice sheet. *PNAS*, 112(4),  
867 1001–1006. doi: 10.1073/pnas.1413024112
- 868 Sommers, A., Rajaram, H., & Morlighem, M. (2018). SHAKTI Subglacial Hydrol-  
869 ogy and Kinetic, Transient Interactions v1.0. *Geoscientific Model Development*,  
870 11(7), 2955–2974. doi: 10.5194/gmd-11-2955-2018
- 871 Spring, U., & Hutter, K. (1981). Numerical studies of jökulhlaups. *Cold Regions Sci-*  
872 *ence and Technology*, 4(3), 227–244.
- 873 Stevens, L. A., Hewitt, I. J., Das, S. B., & Behn, M. D. (2018). Relationship Be-  
874 tween Greenland Ice Sheet Surface Speed and Modeled Effective Pressure.  
875 *Journal of Geophysical Research: Earth Surface*, 123(9), 2258–2278. doi:  
876 10.1029/2017JF004581
- 877 Stubblefield, A. G., Creyts, T. T., Kingslake, J., & Spiegelman, M. (2019). Model-  
878 ing oscillations in connected glacial lakes. *Journal of Glaciology*, 65(253), 745  
879 – 758. doi: 10.1017/jog.2019.46
- 880 Trunz, C. (2021). *Modeling and Measuring Water Level Fluctuations in the Green-*  
881 *land Ice Sheet: How Moulin Life Cycle and Shape can Inform us on the Sub-*  
882 *glacial Drainage System.* (Doctoral Thesis). University of Arkansas, Fayette-  
883 ville.
- 884 Trunz, C. (2022, March). *cctrunz/ModelRepo\_moulinshapestoragepaper: Release v.2.*  
885 Zenodo. Retrieved 2022-03-08, from <https://zenodo.org/record/6338955>  
886 doi: \ci
- 887 Vallot, J. (1898). Exploration des moulins de la Mer de Glace. *Annales de*  
888 *l'Observatoire météorologique du Mont-Blanc*, 3(1), 183–193.
- 889 van der Veen, C. J. (1998). Fracture mechanics approach to penetration of bot-  
890 tom crevasses on glaciers. *Cold Regions Science and Technology*, 27(3), 213–  
891 223. doi: 10.1016/S0165-232X(98)00006-8
- 892 Vatne, G., & Irvine-Fynn, T. D. L. (2016). Morphological dynamics of an englacial  
893 channel. *Hydrology and Earth System Sciences*, 20(7), 2947–2964. doi: 10  
894 .5194/hess-20-2947-2016
- 895 Werder, M. A., Hewitt, I. J., Schoof, C., & Flowers, G. E. (2013). Modeling chan-  
896 nnelized and distributed subglacial drainage in two dimensions. *Journal of Geo-*  
897 *physical Research: Earth Surface*, 118(4), 2140–2158. doi: 10.1002/jgrf.20146
- 898 Werder, M. A., Schuler, T. V., & Funk, M. (2010). Short term variations of tracer  
899 transit speed on alpine glaciers. *The Cryosphere*, 4(3), 381–396. doi: 10.5194/  
900 tc-4-381-2010
- 901 Wright, P. J., Harper, J. T., Humphrey, N. F., & Meierbachtol, T. W. (2016).  
902 Measured basal water pressure variability of the western Greenland Ice Sheet:  
903 Implications for hydraulic potential: Greenland Ice Sheet Basal Water Pres-

904  
905

sure. *Journal of Geophysical Research: Earth Surface*, 121(6), 1134–1147. doi:  
10.1002/2016JF003819